crystals

MDPI

Article

Crystal Engineering of Cation-Radical Salts with Weakly Coordinating Carbadodecaborate Anions

Emmanuel Adeniyi [1], Matthias Zeller [2] and Sergiy V. Rosokha [1,*]

[1] Department of Chemistry, Ball State University, Muncie, IN 47306, USA
[2] Department of Chemistry, Purdue University, West Lafayette, IN 47907, USA
* Correspondence: svrosokha@bsu.edu

Abstract: An X-ray structural analysis revealed that the salts of N,N,N′,N′-tetramethyl-p-phenylenediamine (TMPD), N-methylphenothiazine (MPTZ), and octamethylbiphenylene (OMB), with dodecamethyl- or hexabromo-substituted carbadodecaborate anions, comprise layers of the (partially) oxidized organic donors separated by sheets of the bulky counter-ions. The cationic layers comprise either well-separated $TMPD^+$ or $MPTZ^+$ cation radicals or π-stacks of partially oxidized OMB moieties consisting of more or less distinct $(OMB)_2^+$ units. Quantum mechanical calculations revealed that the formation of essentially isolated cation-radical or π-bonded associations in the salts with these weakly coordinating anions is correlated with the strength of the multicenter π-bonding between cation radicals. This pancake bonding is determined by the balance of the electrostatic repulsion between cationic counterparts and attractive dispersion and weakly covalent interactions.

Keywords: cation radicals; carbadodecaborate anions; X-ray crystallography; DFT computations; multicenter π-bonding

Citation: Adeniyi, E.; Zeller, M.; Rosokha, S.V. Crystal Engineering of Cation-Radical Salts with Weakly Coordinating Carbadodecaborate Anions. *Crystals* **2023**, *13*, 99. https://doi.org/10.3390/cryst13010099

Academic Editor: Alexander Pöthig

Received: 17 December 2022
Revised: 26 December 2022
Accepted: 1 January 2023
Published: 5 January 2023

1. Introduction

Following the discovery of the (super-)conductive and magnetic properties of the cation-radical salts of some planar organic donors, the preparation and characterization of such compounds became one of the central themes of structural and material chemistry [1–5]. The variation of counter-ions and stoichiometry led to wide-range modifications of the crystal architecture of the salts with a certain cation radical. It allowed modulating the 3D arrangement of the networks formed by the ion-radical species and the strength of their interactions, which is critical for the material-science properties [6–8]. Indeed, the substantial electronic coupling between the π-stacked moieties led to electron delocalization, and the charge carrier's mobility within the array was related to the conduction bandwidth. However, strong π-bonding between a pair of cation radicals can also lead to diamagnetic dimers, and thus, it resulted in non-conducting (insulator) states [7].

Previous studies have mostly focused on the cation radicals of tetrathiafulvalene (TTF) analogs (such as bis(ethylenedithio)tetrathiafulvalene (BEDT-TTF) or tetramethyltetraselenafulvalene (TMTSF)) [9]. While these systems are considered the "brick and mortar of organic electronics", [10] further advances in this area require the development of methods for the preparation of salts with diverse types of species, e.g., planar hydrocarbon- or nitrogen-containing cation radicals [11,12]. Since the latter are frequently more reactive than the tetrathiafulvalene cation radicals, crystal engineering of their salts requires a judicious choice of counter-ions [13]. Weakly coordinating anions (WCA), such as the carbadodecaborate derivatives dodecamethyl-closo-1-carbododecaborate ($Me_{12}CAR^-$) or 7,8,9,10,11,12-hexabromo-closo-1-carbododecaborate (Br_6CAR^-) illustrated in Figure 1, have appeared as very promising building blocks for such materials [14–18].

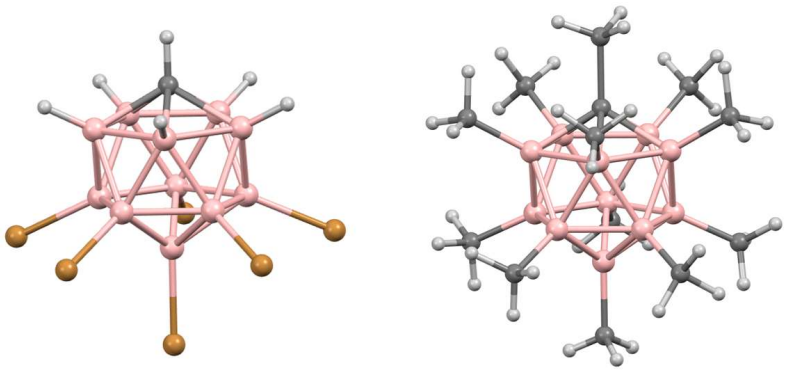

Br_6CAR^- $Me_{12}CAR^-$

Figure 1. Structures and abbreviations of carbadodecaborate anions.

The non-nucleophilic nature of these anions facilitates the stability of the reactive cationic species in the solid state and in solution. Previous works demonstrated that the utilization of these anions allows the preparation of crystalline salts of benzenium, vinyl, or tert-butyl cations, which are persistent at room temperature [19–21]. Carbododecaborate anions were also fruitfully utilized for the isolation of unstable organometallic intermediates [22,23]. Aside from this, the use of bulky anions with delocalized charge allows the electrostatic interactions between counter-ions to be minimized. Therefore, the formation of dimeric (or higher order) associations of cation radicals is predominantly determined by the intrinsic properties of the latter for π-bonding.

We have previously shown that the use of carbadodecaborate anions (Figure 1) allows the preparation of persistent cation-radical salts with targeted stoichiometry and various architectures via chemical oxidation of the neutral tetrathiafulvalene derivatives [24–26]. In particular, the crystalline cation-radical salts with Br_6CAR^- counter-ions were prepared through the interaction of neutral organic donors, D, with tris-(4-bromophenyl)aminium ($TBPA^{+\bullet}$) salts of this anion, $(TPBA)Br_6CAR$, in dichloromethane (Equation (1)):

$$D + (TPBA)Br_6CAR \rightarrow D^{+\bullet} + Br_6CAR^- + TPBA \quad (1)$$

Alternatively, such salts were prepared by the oxidation of donors with the $Me_{12}CAR^{\bullet}$ radical (Equation (2))

$$D + Me_{12}CAR^{\bullet} \rightarrow D^{+\bullet} + Me_{12}CAR^- + TPBA \quad (2)$$

Depending on the donor and stoichiometric ratios of reactants, the structures of these salts comprised isolated cation radicals, dicationic dimers or trimers, or π-stacks of partially oxidized moieties. The variations of the crystal architecture were accompanied by modulation of the spin–spin interactions, and therefore, changes in the magnetic properties of these substances. [25,26] To clarify the applicability and limitations of these synthetic methods, as well as to evaluate the factors determining the crystal architectures of the resulting salts, in the current work, we explored if similar reactions will allow the preparation of cation-radical salts of hydrocarbon or nitrogen-containing donors, such as N,N,N′,N′-tetramethyl-p-phenylenediamine (TMPD), 10-methylphenothiazine (MPTZ), and octamethylbiphenylene (OMB), as shown in Chart 1. Earlier studies indicated the possibility of the formation of π-bonded dimers of these cation radicals [27–29]. As such, we also explored in this work the factors determining the formation of π-bonded associates (which are critical for the properties of the substances) in the salts with minimized interaction with the counter-ions.

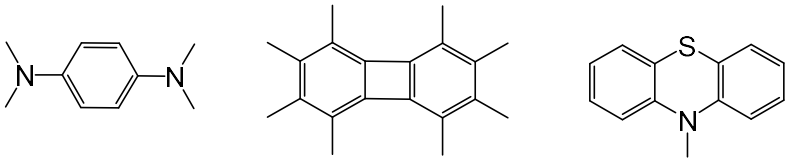

TMPD OMB MPTZ

Chart 1. Structures and abbreviations of the organic donors.

2. Materials and Methods

2.1. Materials

N,N,N′,N′-Tetramethyl-p-phenylenediamine (from Sigma Aldrich, Burlington, MA, USA) was purified by sublimation. 10-Methylphenothiazine, tris(4-bromophenyl)amine (both from Sigma Aldrich, Burlington, MA, USA), cesium dodecamethyl-closo-1-carbododecaborate, $CsMe_{12}CAR$, (from Katchem, Praha, Czech Republic), and silver 7,8,9,10,11,12-hexabromo-closo-1-carbododecaborate, $AgBr_6CAR$ (from Strem, Newburyport, MA, USA) were used without additional purification. Octamethylbiphenylene was prepared by the reaction of 1,2-dibromotetramethylbenzene with n-butyl lithium (both from Sigma Aldrich, Burlington, MA, USA) [30]. Dodecamethylcarboranyl radicals, $Me_{12}CAR^{\bullet}$, were prepared by the reaction of $CsMe_{12}CAR$ with PbO_2 in acetonitrile [31]. $(TBPA)Br_6CAR$, was synthesized by the addition of Br_2 to a solution of $AgBr_6CAR$ and TBPA in anhydrous dichloromethane under an N_2 atmosphere at −78 °C, as described earlier [32]. A similar reaction using half of the stoichiometric ratio of Br_2 resulted in the formation of $(TBPA)Ag(Br_6CAR)_2$. The purity of these salts (>98%) was confirmed via UV–vis measurements (using the characteristic absorption band of the $TBPA^{+\bullet}$ cation radical at λ_{max} = 704 nm with $\varepsilon = 3.3 \times 10^4$ $M^{-1}cm^{-1}$ [32]).

2.2. Crystallization and X-ray Structural Analysis

The cation-radical salts with $Me_{12}CAR^{-}$, Br_6CAR^{-} or $Ag(Br_6CAR)_2^{-}$ counter-ions were prepared by the addition of a solution of either $AgBr_6CAR$, $(TBPA)Br_6CAR$ or $CAR^{\bullet}$ to the dichloromethane solutions of the organic donors under an argon atmosphere. The addition of hexane and partial evaporation of dichloromethane led to the formation of dark-colored crystalline salts of the cation radicals. These salts were recrystallized by slow evaporation of their solutions in dichloromethane:hexane (5:1) mixtures or from acetonitrile. Such recrystallizations produced crystals suitable for X-ray crystallography analysis. The purity of the salts (>97%) was established using UV–vis spectral measurements by comparison of the intensities of the absorption maxima of the solutions prepared from the bulk samples with those predicted based on the characteristic absorption bands of the corresponding cation radicals in the visible range [27–29,32]. The FT-IR spectra of the cation-radical salts and parent neutral molecules are shown in Figures S1–S3 in the Supporting Information.

Specifically, to prepare $(TMPD)Br_6CAR$, 66 mg (0.060 mmol) of $(TBPA)Br_6CAR$ in 5 mL CH_2Cl_2 was added to a solution of 17.0 mg (0.10 mmol) of TMPD in 5 mL of CH_2Cl_2 in a Schlenk tube under argon atmosphere. After the mixture was stirred for 10 min, 10 mL of hexane was added and about 60% of the solution was evaporated under reduced pressure. The dark precipitate was filtered off, washed with pentane, and dried under vacuum (45 mg, yield 82%). This material was dissolved in 10 mL of a 2:1 dichloromethane/hexane mixture. Slow evaporation of this solution resulted in the formation of dark plates of $(TMPD)Br_6CAR$ suitable for a single crystal X-ray analysis (vide infra). $(MPTZ)Br_6CAR$ and $(OMB)_2Br_6CAR$ salts were prepared in a similar way through the interaction of 20 mg (0.090 mmol) of MPTZ or 24 mg (0.091 mmol) of OMB with 66 mg (0.060 mmol) of $(TBPA)Br_6CAR$. $(OMB)_2[Ag(Br_6CAR)_2]$ was prepared by mixing the solutions of 14.5 mg (0.055 mmol) of OMB with 44.3 mg (0.024 mmol) of $TBPA[Ag(Br_6CAR)_2]$. To prepare $(TMPD)Me_{12}CAR$, a solution of 13 mg (0.042 mmol) of $CAR^{\bullet}$ in pentane was added to the solution of 7.1 mg (0.043 mmol) of TMPD in 5 mL of CH_2Cl_2 in a Schlenk tube, and the solution was stirred for 10 min.

Hexane (20 mL) was added to this solution, and about 60% of the solution was evaporated under reduced pressure. The dark (TMPD)Me_{12}CAR precipitate was filtered off, washed with pentane, and dried. (MPTZ)Me_{12}CAR was similarly prepared by the interaction of 13 mg (0.042 mmol) of CAR$^{\bullet}$ with 10.0 mg (0.045 mmol) of MPTZ.

The single crystal structures of all salts except (TMPD)Me_{12}CAR were examined on a Bruker Quest diffractometer (Bruker AXS, LLC, Madison, WI, USA)with a fixed chi angle, a sealed tube fine-focus X-ray tube, a single crystal curved graphite incident-beam monochromator (Bruker AXS, LLC, Madison, WI, USA), and a Photon100 or PhotonII area detector (Bruker AXS, LLC, Madison, WI, USA). Examination and data collection were performed with Mo Kα radiation (λ = 0.71073 Å). A single crystal of (TMPD)Me_{12}CAR was analyzed with a Bruker Quest diffractometer (Bruker AXS, LLC, Madison, WI, USA) with a PhotonII area detector with microsource Cu Kα radiation (λ = 1.54178 Å). Both instruments were equipped with an Oxford Cryosystems low-temperature device, and all data were collected at 150 K. Reflections were indexed and processed, and the files were scaled and corrected for absorption using APEX3 or APEX4 [33]. The space groups were assigned using XPREP within the SHELXTL suite of programs [34], and the structures were solved by direct or dual space methods and refined by full-matrix least-squares against F^2 with all reflections using Shelxl2018 [35,36], using the graphical interface Shelxle [37].

(TMPD)Br_6CAR (1). Chemical formula $C_{11}H_{22}B_{11}Br_6N_2$, M = 780.67 g/mol. Orthorhombic, space group *Pnma*, a = 12.2897 (17) Å, b 19.147 (3) Å, c = 10.683 (2) Å, V = 2513.7 (7) Å^3, Z = 4, T = 150 K, μ(Mo *K*α) = 9.59 mm^{-1}, 25,820 reflections measured, 4301 unique (R_{int} = 0.084). The final R1 was 0.033 (I > 2σ(I)) and wR2 was 0.080 (all data).

(TMPD)Me_{12}CAR (2). Chemical formula $C_{23}H_{52}B_{11}N_2$, M = 475.57 g/mol. Monoclinic, space group $P2_1/c$, a = 9.4382 (5) Å, b = 16.2939 (8) Å, c = 10.0320 (5) Å, β = 99.988 (2)°, V = 1519.39 (13) Å^3, Z = 2, T = 150 K, μ(CuKα) = 0.38 mm^{-1}, 23,308 reflections measured, 5240 unique (R_{int} = 0.078). The final R1 was 0.069 (I > 2σ(I)) and wR2 was 0.206 (all data).

(MPTZ)Br_6CAR·CH_2Cl_2 (3). Chemical formula $C_{15}H_{29}B_{11}Br_6$ Cl_2NS, M = 914.64 g/mol. Monoclinic, space group $P2_1/c$, a = 14.5114 (6) Å, b = 11.9307 (5) Å, c = 17.2932 (7) Å, β = 92.143 (3)°, V = 2991.9 (2) Å^3, Z = 4, T = 150 K, μ(Mo *K*α) = 8.31 mm^{-1}, 67,062 reflections measured, 8757 unique (R_{int} = 0.117). The final R1 was 0.045 (I > 2σ(I)) and wR2 was 0.116 (all data).

(MPTZ)Me_{12}CAR (4). Chemical formula $C_{13}H_{47}B_{11}NS$, M = 524.61 g/mol. Triclinic, space group $P\bar{1}$, a = 9.1947 (7) Å, b 9.6197 (7) Å, c = 9.8672 (6) Å, α = 92.220 (4)°, β = 108.427 (4)°, γ = 107.029 (4)°, V = 783.37(10) Å^3, Z = 1, T = 150 K, μ(Mo *K*α) = 0.102 mm^{-1}, 31,192 reflections measured, 5974 unique (R_{int} = 0.046). The final R1 was 0.058 (I > 2σ(I)) and wR2 was 0.188 (all data).

$(OMB)_2Br_6$CAR·CH_3CN (5). Chemical formula $C_{43}H_{57}B_{11}Br_6N$, M = 1186.26 g/mol. Monoclinic, space group $P2_1/m$, a = 8.5334 (10) Å, b = 28.567 (2) Å, c = 10.1051 (9) Å, β = 102.614 (6)°, V = 2403.9 (4) Å^3, Z = 2, T = 150 K, μ(Mo *K*α) 5.04 mm^{-1}, 30,815 reflections measured, 5940 unique (R_{int} = 0.070). The final R1 was 0.060 (I > 2σ(I)) and wR2 was 0.134 (all data).

$(OMB)_2$·[Ag(Br_6CAR)$_2$ ·CH_2Cl_2 (6). Chemical formula $C_{44}H_{64}AgB_{22}$ $Br_{12}Cl_4$, M = 2039.24 g/mol. Triclinic, space group $P\bar{1}$, a = 7.4994 (11) Å, b = 14.880 (2) Å, c = 16.050 (2) Å, α = 79.284 (6)°, β = 84.942 (6)°, γ = 81.080 (6)°, V = 1735.2 (4) Å^3, Z = 1, T = 150 K, μ(Mo *K*α) 7.39 mm^{-1}, 58,189 reflections measured, 13,229 unique (R_{int} = 0.054). The final R1 was 0.040 (I > 2σ(I)) and wR2 was 0.105 (all data).

Details of the refinement of disorders or twinning in structures 2, 4 and 5 are presented in the Supporting Information. Complete crystallographic data, in CIF format, have been deposited with the Cambridge Crystallographic Data Centre. CCDC 2224556–2224561 contain the supplementary crystallographic data for this paper. These data can be obtained free of charge via www.ccdc.cam.ac.uk/data_request/cif (accessed on 15 December 2022).

2.3. Computations

Geometries of the monomers and dimers were optimized without constraints via DFT calculations with the UM06L functional and a def2tzvpp basis set using the Gaussian 09 suite of programs [38,39]. Previous work showed that these methods provide a good model for π-bonded associations of ion radicals at a reasonable computational cost [40]. Moreover, the use of UM06L/def2tzvpp calculations in acetonitrile and/or dichloromethane allows comparing the stabilities of the π-bonded dimers of the cation radicals of OMB, TMPD, and MPTZ with those formed by the TTF derivatives which we reported earlier [25,26]. Calculations with acetonitrile or dichloromethane as a medium were carried out using a polarizable continuum model [41]. The absence of imaginary frequencies confirmed that the optimized structures represent true minima. Values of the formation energies, ΔE, of the dicationic dimers were determined as: $\Delta E = E_{dim} - 2E_{CR}$, where E_{dim} and E_{CR} are the energies (including ZPE) of the optimized dimers and monomer cation radicals, respectively. The ΔE values for the monocationic dimers were determined as: $\Delta E = E_{dim} - E_{CR} - E_N$, where E_N is the energy of the optimized neutral organic donor. The energies of dimeric and monomeric species are listed in Table S1 in the Supporting Information. ΔE values in dichloromethane and vacuum were estimated in the same way using energies obtained via single-point calculations, using coordinates of the species optimized in acetonitrile. The singlet–triplet energy gap, ΔE_{TS}, was determined as the difference in the energies of the optimized dimers in their (ground-state) singlet states and the energies of the triplet states obtained via single-point calculations using the same geometry [42]. Following Winter et al. [43], the dispersion components, E_{DIS}, were estimated as the difference between the energies of the calculated dimers (with the def2tzvpp basis set and the geometries obtained from the UM06L optimizations), using the B97D functional (which includes a dispersion correction) and the B98 functional (without dispersion correction), $E_{DIS} = \Delta E(B98) - \Delta E(B97D)$, (Table S2 in the Supporting Information). The electrostatic interaction energies between monomers in the dimers were estimated by summarizing the electrostatic interaction (in vacuum) between the charges located at the positions of each atom of one of the monomers and the charges located at the positions of each atom of their counterparts (i.e., summation is limited to atomic pairs that belong to different monomers): $E_{ES} = \frac{1}{2}\sum_i \sum_j kq_iq_j/r_{ij}$, where k is the Coulomb constant, q_i and q_j are the values of charges (calculated as the ESP charges) of the atoms in two monomers, and r_{ij} are distances between these atoms calculated from their coordinates in the dimers ($\frac{1}{2}$ coefficient is included to avoid double-counting of interactions between each pair of atoms (Table S3 in the Supporting Information)). The quantum theory of atoms in molecules (QTAIM) and non-covalent indices (NCI) analyses were performed with the Multiwfn program [44]. They were visualized using the VMD program [45].

3. Results and Discussion

3.1. X-ray Structural Characterization of the Cation-Radical Salts

The addition of a colorless solution of an organic donor D from Chart 1 in dichloromethane to the solutions of (TBPA)Br_6CAR or $CAR^{\bullet}$ resulted in the rapid change of color of the mixture. UV-vis spectral measurements indicated that these changes are related to the disappearance of the strong absorption band of the $TBPA^{+\bullet}$ cation radical at 704 nm, or the weak band of $CAR^{\bullet}$ at 900 nm, and the formation of the bands of the corresponding cation radicals $D^{+\bullet}$. The addition of hexane and partial evaporations of the solutions resulted in the precipitation of the salts of $D^{+\bullet}$ with Br_6CAR^{-} or CAR^{-} in an essentially quantitative yield. Recrystallization of the salts from dichloromethane/hexane mixtures produced crystalline materials suitable for a single-crystal X-ray structural analysis.

In particular, the X-ray analysis revealed that the oxidation of TMPD with $CAR^{\bullet}$ radicals produced monoclinic crystals ($P2_1/c$ space group) of (TMPD)Me_{12}CAR. This salt comprised layers of $Me_{12}CAR^{-}$ anions and $TMPD^{+}$ cation radicals parallel to the *bc* plane (Figure 2A).

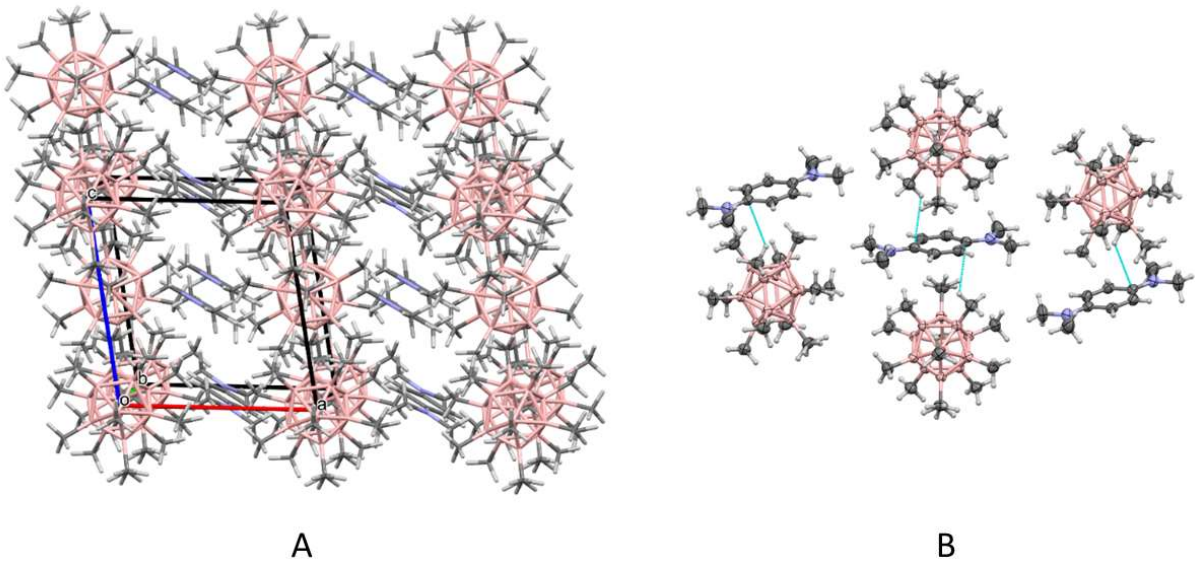

Figure 2. The crystal lattice of (TMPD)Me_{12}CAR (**A**) comprising essentially isolated $TMPD^{+\bullet}$ cation radicals (**B**). Light blue lines indicate contacts shorter than the van der Waals separations.

The center-to-center distance between TMPD moieties in these layers is large (9.43 Å), and they are surrounded by the Me_6CAR^- counter ions. As such, there are no short contacts between essentially isolated $TMPD^{+\bullet}$ moieties. Average bond lengths within practically planar (centrosymmetric) $TMPD^{+\bullet}$ in this salt are listed in Table 1. The comparison of their values with the reported earlier characteristics of the corresponding neutral molecule [46] showed that the bonds adjacent to the amino-substituents (designated as b) became longer, while bonds designated a became shorter than that in the neutral molecule (which shows all bonds within the aromatic ring in the 1.39 ± 0.01 Å range). The C-N bond lengths were also about 0.06 Å shorter than that in the neutral molecules. All these differences are consistent with the structural features of earlier reported $TMPD^{+\bullet}$, and they indicate that oxidation led to a substantial quinonoidal distortion of the aromatic TMPD moieties.

Table 1. Average bond length (in Å) in the D cores in the salts with WCA counter-ions.

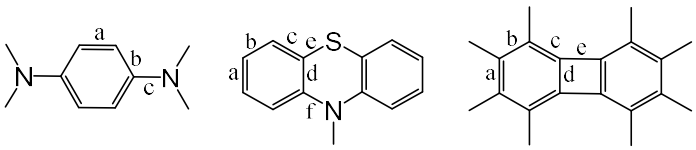

Salt [i]	a [ii]	b [ii]	c [ii]	d [ii]	e [ii]	f [ii]
(TMPD)Me_{12}CAR	1.357	1.421	1.342	1.453		
(TMPD)Br_6CAR	1.354	1.424	1.350	1.460		
(MPTZ)Br_6CAR	1.403	1.359	1.408	1.393	1.723	1.391
(MPTZ)Me_{12}CAR [iii]	1.399	1.366	1.408	1.411	1.715	1.389
$(OMB)_2Br_6$CAR	1.421	1.422	1.376	1.434	1.501	
$(OMB)_2[Ag(Br_6CAR)_2]$	1.418	1.422	1.378	1.426	1.4915	

[i] Solvate molecules are not listed. [ii] See the structures above. [iii] Disordered MPTZ moiety.

Oxidation of the same TMPD molecules with $TBPA^{+\bullet}$, taken as a salt with Br_6CAR^- anions (Equation (1)), produced orthorhombic crystals of (TMPD)Br_6CAR. They contain layers of $TMPD^{+\bullet}$ and Br_6CAR^- moieties parallel to an *ac* plane (Figure S4 in the Supporting Information). Similar to (TMPD)Me_{12}CAR crystals, $TMPD^{+\bullet}$ cation radicals are substantially separated from each other (with a center-to-center distance of 8.14 Å) and show short contacts only with Br_6CAR^- anions. The geometric characteristics of the essentially planar $TMPD^{+\bullet}$ were also quite close to those in the (TMPD)Me_{12}CAR salt (Table 1).

The crystallization of N-methylphenothiazine cation radicals with Br_6CAR^- anions produced monoclinic crystals in the $P2_1/c$ space group. The X-ray structural analysis showed that these crystals comprised double chains of $MPTZ^{+\bullet}$ moieties surrounded by Br_6CAR^- anions (Figure 3A). These double chains consist of parallel rows of $MPTZ^{+\bullet}$ cations arranged at a distance of about 3.2 Å (Figure 3B).

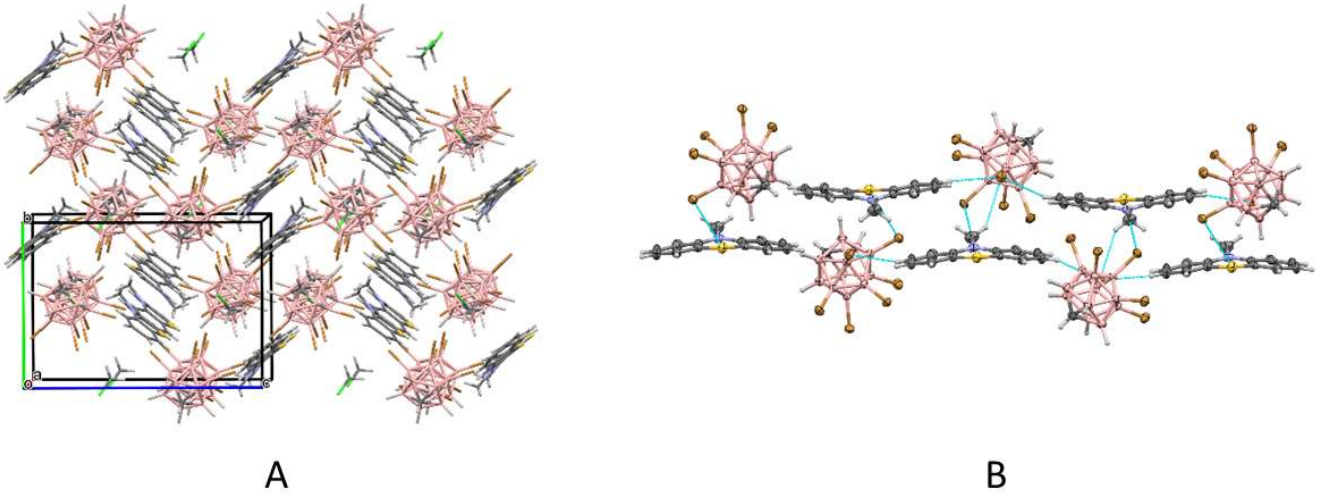

Figure 3. The crystal lattice of (MPTZ)Br_6CAR (**A**) comprising essentially isolated $MPTZ^{+\bullet}$ cation radicals (**B**). Light blue lines indicate contacts shorter than the van der Waals separations.

The $MPTZ^{+\bullet}$ cations in one of the rows were turned by 180° and shifted by 4.7 Å with respect to the moieties in the other row, so a central N-S axis of a molecule in one row was located above the gap between two molecules in the other row. As a result, the aromatic rings of the $MPTZ^{+\bullet}$ moieties in one row were stacked over the aromatic rings of two of their counterparts in the other row. However, no contacts were shorter than the van der Waals separations between $MPTZ^{+\bullet}$ in the same or different rows. A comparison of the geometry of the cationic and neutral MPTZ showed that the angle between rings of 14.5° in the cation radical is much smaller than that in the neutral molecule (36.3°) [47]. The geometric characteristics listed in Table 1 also indicate that besides substantial planarization of the MPTZ moiety, its oxidation led to the shortening of S-C and N-C bonds in the central ring. Moreover, the side (aromatic) rings became more distorted, with bonds designated b being noticeably shorter than the other bonds.

The interaction of MPTZ with $Me_{12}CAR^{\bullet}$ radicals produced triclinic crystals in the space group $P\bar{1}$. Similar to the salt with Br_6CAR^-, these crystals comprised layers of $MPTZ^{+\bullet}$ separated by sheets of $Me_{12}CAR^-$ (Figure S5A in the Supporting Information). In this case, the $MPTZ^{+\bullet}$ were disordered. Most notably, they were also arranged at significant separations from each other (with the center-to-center distance between neighboring moieties of more than 9 Å). As such, no π-stacking was observed, and there were short contacts only between the side carbon atoms in the MPTZ aromatic rings (Figure S5B in the Supporting Information).

In contrast to the reactions with TMPD or MPTZ, the interaction of (TBPA)Br_6CAR with OMB resulted in the crystallization of a salt with 2:1 OMB to Br_6CAR stoichiometry. The X-ray analysis showed that the monoclinic $(OMB)_2Br_6CAR$ crystals (obtained by slow cooling of their solution in acetonitrile from room temperature to −30 °C) comprised layers of cationic OMB moieties separated by layers of anions and molecules of acetonitrile (Figure 4A).

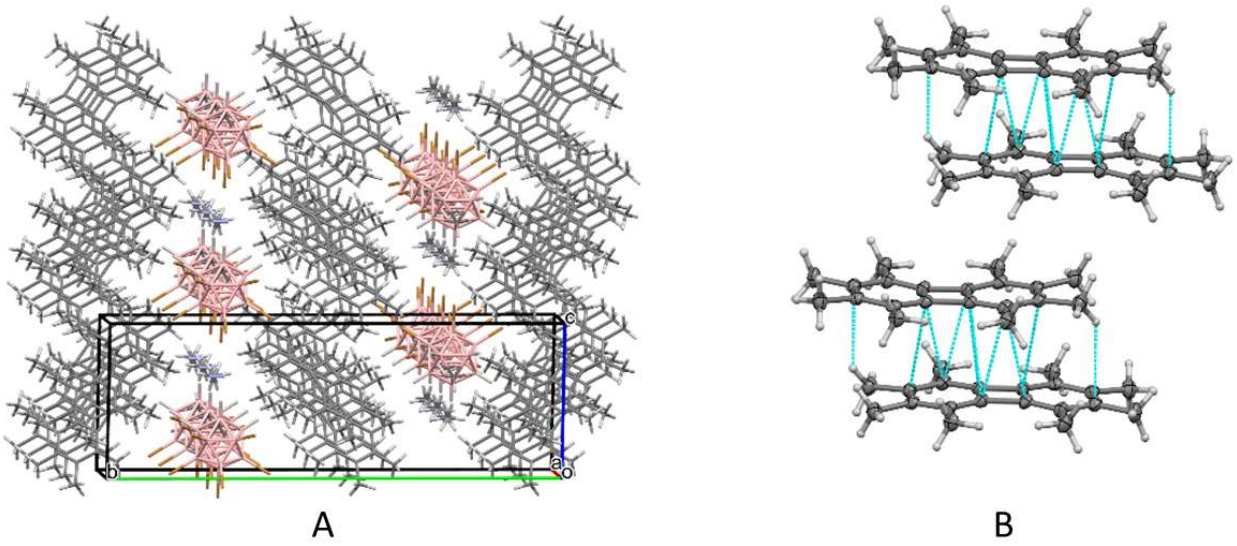

Figure 4. Crystal lattice of $(OMB)_2Br_6CAR$ (**A**) comprising stacks of partially oxidized OMB moieties (**B**). Light blue lines indicate contacts shorter than the van der Waals separations.

The cationic layers showed stacks of co-planar OMB moieties consisting of distinct centrosymmetric pairs of partially oxidized electron donors. The interplanar distance between OMB moieties in these dyads of 3.38 Å was noticeably smaller than the distance of 3.58 Å between molecules from the neighboring pairs. Moreover, the OMB molecules slightly deviated from planarity, and their central parts were shifted towards each other. Accordingly, the pairs showed multiple intermolecular C-C distances (shown as blue lines in Figure 4B), which were shorter than the sum of the van der Waals radii of carbons of 3.40 Å (with the shortest C-C separation being 3.292 Å). In comparison, there were no such short separations between OMB molecules from the neighboring dyads. All these data indicate that multicenter π-bonding (referred to as pancake bonding [48–50]) between neighboring species resulted in the formation of distinct monocationic dimers. Furthermore, the stoichiometry of the salt and symmetry of the paramagnetic $(OMB_2)^{+\bullet}$ pairs (which are frequently called "pimers" [51]) indicate that positive charge was delocalized over both OMB moieties. In accordance with these 0.5+ charges, the average bond lengths of the OMB cores in Table 1 are intermediate between those in the reported neutral molecule and its cation radical.

The crystals resulting from the oxidation of OMB with $Me_{12}CAR^{\bullet}$ radicals were not suitable for the X-ray structural analysis. Thus, to verify the generality of the formation of π-stacks of OMB moieties showing pancake bonding in the salts with bulky weakly coordinating anions, the salt of $TPBA^{+\bullet}$ with $Ag(Br_6CAR)_2^-$ anions was prepared (see Materials and Methods for details). Interaction of this oxidant with octamethylbiphenylene produced a salt comprising OMB and $Ag(Br_6CAR)_2^-$ in a 2:1 stoichiometry. The X-ray structural analysis revealed that the triclinic crystals of this salt contain layers of OMB molecules together with CH_2Cl_2 solvate (Figure 5A). They were separated by layers of anionic $[Ag(Br_6CAR)_2]$ complexes (consisting of two Br_6CAR anions coordinated via three of their bromine substituents to silver cations, similar to the earlier reported complex [52].

Similar to the $(OMB)_2Br_6CAR$ salt, the OMB layers comprised stacks of co-planar OMB moieties, in which the neighbors were shifted relative to each other by about 1.5 Å. Their identical geometries indicate an equal +0.5 charges on each OMB moiety. The average bond lengths within the OMB core were also intermediate between those in the neutral and monocationic species, and they were close to those in the salt with Br_6CAR^- anions. The interplanar separations between the OMB molecule and its two neighbors of about 3.47 Å and 3.60 Å were also somewhat different. However, since the smaller of these separations was more than 3.40 Å, no intermolecular C-C contacts were shorter than the sum of the van der Waals radii.

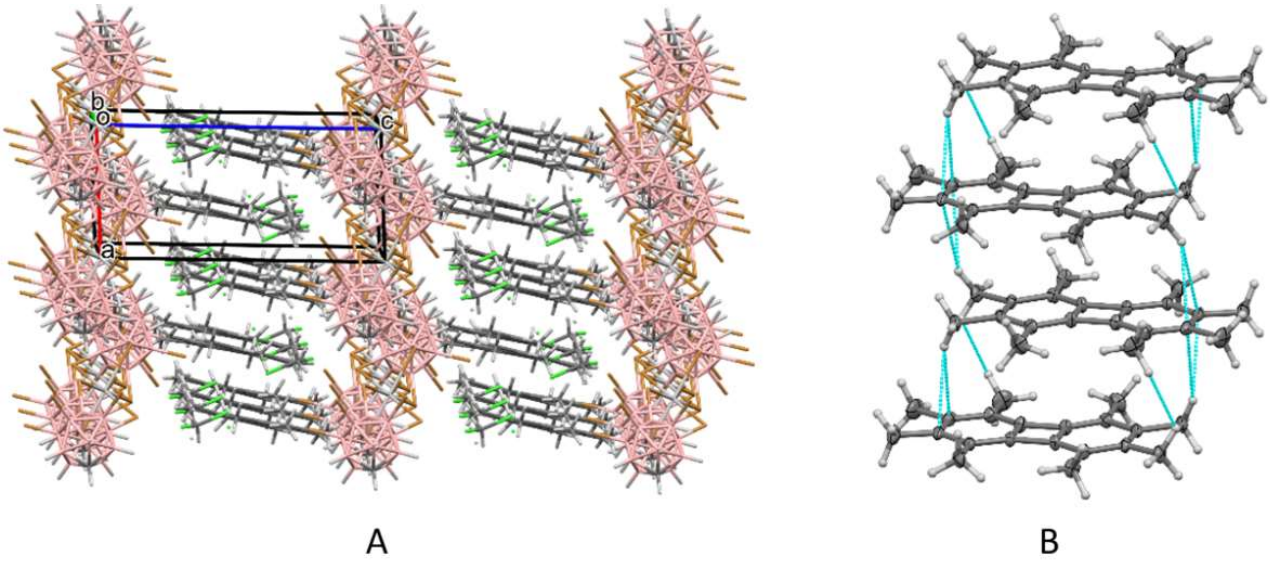

Figure 5. The crystal lattice of $(OMB)_2$ $[Ag(Br_6CAR)_2]$ (**A**) comprising stacks of partially oxidized OMB moieties (**B**). Light blue lines indicate contacts shorter than the van der Waals separations.

3.2. Quantum-Mechanical Computations of the Dimers of Cation Radicals

To evaluate reasons for the crystallization of the π-bonded associations or essentially isolated cation radicals, we employed quantum-mechanical calculations of the $TMPD_2^{2+}$, $MPTZ_2^{2+}$, and OMB_2^{2+} dimers. The UM06L/def2tzvpp calculations (with acetonitrile as medium) produced stable π-bonded dimers. The structures of these dicationic associations are illustrated in Figure 6.

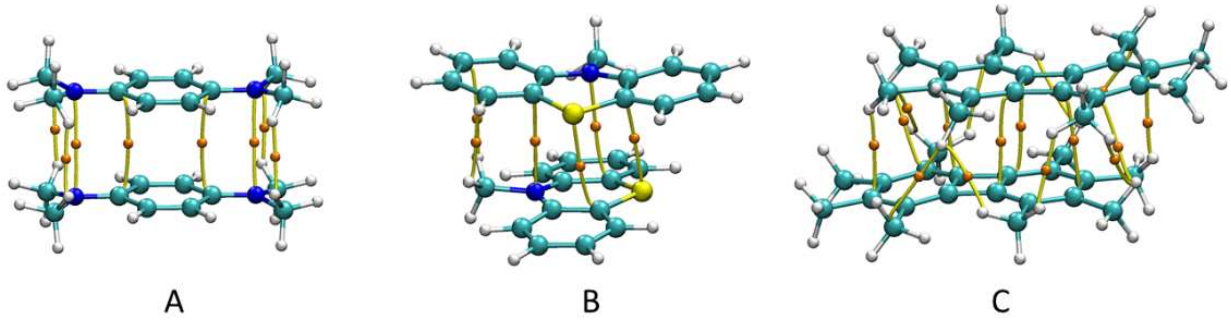

Figure 6. Optimized structures of $TMPD_2^{2+}$ (**A**), $MPTZ_2^{2+}$ (**B**) and OMB_2^{2+} (**C**) dimers showing bond critical points (small orange spheres) and bond paths (orange lines) between cationic fragments (from QTAIM analysis).

The $TMPD_2^{2+}$ dyad showed two co-planar TMPD moieties, shifted relative to each other perpendicular to their main axes (the dimer in which counterparts were shifted parallel to the main axes showed somewhat higher energy). The interplanar separation was about 3.15 Å, and there were a number of interatomic C-C distances of about 3.20 Å (which are shorter than the sum of the van der Waals separations of 3.40 Å for carbon atoms). The $MPTZ^{2+}$ dimer comprised two molecules turned about 90° relative to each other (a similar crossed decker arrangement was observed earlier in the dicationic trimers of thianthrene [53]). These dimers also showed several S-C contacts in the 3.15–3.30 Å range (which are shorter than the corresponding sum of the van der Waals radii of 3.50 Å [54]). The OMB_2^{2+} dimer consisted of two moieties shifted relative to each other along their main axes. This dimer also showed multiple C-C contacts in the 3.0–3.2 Å range. Such arrangements of monomers in all three dimers suggests strong pancake bonding between the π-stacked cationic moieties. The QTAIM analysis revealed multiple (3,−1) bond critical points (BCPs) and the corresponding bond paths between the counterparts corrob-

orating such a multicenter π-bonding (electron densities at the BCPs along bond paths connecting two fragments are listed in Table S5 in the Supporting Information). The interaction energy values resulting from the M062X/def2tzvpp calculations of these dimers are listed in Table 2.

Table 2. Formation energies and its components (in kJ/mol) of the calculated π-dimers.

π-Dimer	ΔE [a]	E_{ST} [b]	E_{disp} [c]	E_{ES} [d]
$TMPD_2^{2+}$	−14.5	−34.0	−101.9	245.8
$MPTZ_2^{2+}$	−30.7	−37.2	−92.8	239.0
OMB_2^{2+}	−74.0	−71.5	−177.0	216.7

[a] From M062X/def2tzvpp calculations, with CH_3CN as the medium. [b] Singlet–triplet energy gap. [c] Dispersion interaction. [d] Electrostatic interaction between monomers in the π-dimers (see Materials and Methods and Supplementary Information for details).

The ΔE values in Table 2 indicate that the OMB_2^{2+} dimers are substantially more stable than their $TMPD_2^{2+}$ or $MPTZ_2^{2+}$ analogs. Comparison with the values (calculated in the same way) reported earlier for π-dimers of the tetrathiafulvalene derivatives and the crystal structures of their cation radicals [25,26] demonstrated that the formation of the π-bonded associations in salts with the weakly coordinating anions is highly correlated with the strength of pancake bonding. Indeed, the bonding involving $TMPD^{+\bullet}$ or $MPTZ^{+\bullet}$ was weaker than that reported earlier between $TTF^{+\bullet}$ cation radicals (which show ΔE of −38.9 kJ/mol). Accordingly, similar to the TTF, salts of TMPD and MPTZ with weakly-coordinating $Me_{12}CAR^-$ and Br_6CAR^- anions comprised isolated cation radicals. The ΔE values for the OMB_2^{2+} dimers were more negative than those determined for analogous BEDT-TTF_2^{2+} or $TMTSF_2^{2+}$ dyads (−60.2 and −67.7 kJ/mol, respectively [25]). In agreement with the strong pancake bonding, the salts of all these derivatives with Br_6CAR^- or $Me_{12}CAR^-$ (or other weakly-coordinating anions) comprised π-bonded associations.

To establish the reasons for the differences in strength of the pancake bonding of cation radicals of TMPD, MPTZ, and OMB (and therefore the crystal architectures of their salts), we estimated electrostatic, dispersion and weakly covalent components in their interactions. The data in Table 2 show that while electrostatic repulsion between cationic counterparts in these associations is comparable, the dispersion interaction in OMB_2^{2+} dimers was higher than in its TMPD and MPTZ analogs. Moreover, the difference in energy between triplet and singlet states in the OMB_2^{2+} associations (which reflects the strength of molecular–orbital interaction [42]) was also much larger than that in the $TMPD_2^{2+}$ or $MPTZ_2^{2+}$ analogs. Thus, more favorable dispersion and molecular–orbital interactions result in the substantially higher strength of the pancake bonding involving the OMB cation radicals.

Finally, to determine the reason for the formation of the $(OMB)_2^{+\bullet}$ associations (all salts were prepared under the condition of an excess of organic donors), we compared the stability of the monocationic and dicationic dimers of OMB. The ΔE values for these associations resulting from calculations with polar acetonitrile as a medium were similar. However, earlier studies demonstrated that the magnitudes of the (negative) ΔE values for the dicationic dimers in moderately polar dichloromethane are substantially smaller than those in acetonitrile, and they become positive if calculations are carried out in vacuum [26]. The dicationic dimers under study in the current work showed similar tendencies (Table S4 in the Supporting Information). In comparison, the changes in the ΔE values for monocationic dimers with polarity of the medium were much smaller, and these associations remained stable even in vacuum. Apparently, the environment in the salts with the weakly coordinating anions is best modeled by the relatively low-polar solvents; therefore, it is best suited for the formation of monocationic $(OMB)_2^{+\bullet}$ associations.

4. Conclusions

The electrostatic interaction between counter-ions is a dominant factor in the formation of the ionic compounds, and it plays an essential role in their crystal architectures.

Therefore, the variation of counter-ions frequently (and unpredictably) led to a switch from the crystallization of isolated ion radicals to the formation of the π-dimers. The use of weakly coordinated anions allowed minimizing such electrostatic forces. As a result, the appearance of the π-bonded associations in the WCA salts with the variety of cation radicals was determined by the strength of the pancake bonding of the latter. Indeed, the six salts prepared in the current work showed similar layers of oxidized donors separated by layers of bulky anions. However, while the layers of TMPD and MPTZ salts comprised practically isolated cation radicals, the OMB salts contained π-stacked associations. A similar switch from the crystallization of the isolated cation radical to the formation of the solid-state dimer with the increase in the strength of the (calculated) pancake bonding was observed earlier in the salts of WCA with the oxidized TTF derivatives. The identification of such trends allows targeted preparation of the salts with the distinct arrangements of ion radicals, thus, enabling exploration of the effects of the wide variations of interaction between them on the spectral, conducting, and magnetic properties of these solid-state materials.

Supplementary Materials: The following are available online at https://www.mdpi.com/article/10.3390/cryst13010099/s1: Details of X-ray structures' analysis; Figures S1–S3: FT-IR spectra; Figure S4: X-ray structure of (TMPD)Br_6CAR; Figure S5: X-ray structure of (MPTZ)Me_{12}CAR; Table S1: Calculated energies of the monomers and dimers; Table S2: Details of calculations of dispersion; Table S3: Coordinates and atomic charges; Table S4: Energies of the π-bonded dimers calculated in vacuum and in dichloromethane; Table S5: Electron density at the BCPs in the π-bonded dimers.

Author Contributions: Conceptualization and methodology, S.V.R.; crystal preparation, E.A.; X-ray crystallographic analysis, M.Z.; quantum mechanical computations and data analysis, visualization, S.V.R.; writing—original draft preparation, S.V.R.; writing—review and editing, E.A., M.Z. and S.V.R.; supervision, S.V.R.; funding acquisition, S.V.R. and M.Z. All authors have read and agreed to the published version of the manuscript.

Funding: This research was funded by the Petroleum Research Fund of the American Chemical Society (grant 56516-UR). X-ray structural measurements were supported by the National Science Foundation through the Major Research Instrumentation Program under Grant No. CHE 1625543 (funding for the single crystal X-ray diffractometer). Calculations were performed on Ball State University's Beowulf cluster, which is supported by the National Science Foundation (MRI-1726017) and Ball State University.

Institutional Review Board Statement: Not applicable.

Informed Consent Statement: Not applicable.

Data Availability Statement: Crystallographic data have been deposited with the Cambridge Crystallographic Data Centre and can be obtained free of charge (see above). Atomic coordinates and energies of the calculated complexes are available in the Supplementary Information.

Acknowledgments: We thank S. Dunlap and C. Kunk for the synthesis of OMB.

Conflicts of Interest: The authors declare no conflict of interest.

References

1. Wudl, F.; Wobschall, D.; Hufnagel, E.J. Electrical conductivity by the bis(1,3-dithiole)-bis(1,3-dithiolium) system. *J. Am. Chem. Soc.* **1972**, *94*, 670–672. [CrossRef]
2. Coleman, L.B.; Cohen, M.J.; Sandman, D.J.; Yamagishi, F.G.; Garito, A.F.; Heeger, A.J. Superconducting fluctuations and the Peierls instability in an organic solid. *Solid State Commun.* **1973**, *12*, 1125–1132. [CrossRef]
3. Miller, J.S. Organometallic and Organic-based magnets: New chemistry and new materials for the new millennium. *Inorg. Chem.* **2000**, *39*, 4392–4408. [CrossRef]
4. Williams, J.M. *Organic Superconductors: Synthesis, Structure, Properties and Theory*; Prentice Hall: Englewood Cliffs, NJ, USA, 1992.
5. Miller, J.S.; Drillon, M. (Eds.) *Magnetism: Molecules to Materials*; Wiley-VCH: Weinheim, Germany, 2001.
6. Deumal, M.; Vela, S.; Fumanal, M.; Ribas-Arino, J.; Novoa, J.J. Insights into the magnetism and phase transitions of organic radical-based materials. *J. Mater. Chem. C* **2021**, *9*, 10624–10646. [CrossRef]
7. Bredas, J.L.; Calbert, J.P.; da Silva Filho, D.A.; Cornil, J. Organic semiconductors: A theoretical characterization of the basic parameters governing charge transport. *Proc. Nat. Acad. Sci. USA* **2002**, *99*, 5804. [CrossRef]

8. Giamarchi, T. Theoretical framework for quasi-one dimensional systems. *Chem. Rev.* **2004**, *104*, 5037–5056. [CrossRef] [PubMed]
9. Yamada, J.-I.; Sugimoto, T. *TTF-Foreword. TTF Chemistry: Fundamentals and Applications of Tetrathiafulvalene*; Springer: New York, NY, USA, 2004.
10. Bendikov, M.; Wudl, F.; Perepichka, D.F. Tetrathiafulvalenes, oligoacenenes, and their Buckminsterfullerene derivatives: The brick and mortar of organic electronics. *Chem. Rev.* **2004**, *104*, 4891. [CrossRef]
11. Chi, X.; Itkis, M.E.; Kirschbaum, K.; Pinkerton, A.A.; Oakley, R.T.; Cordes, A.W.; Haddon, R.C. Dimeric phenalenyl-based neutral radical molecular conductors. *J. Am. Chem. Soc.* **2001**, *123*, 4041–4048. [CrossRef]
12. Enkelmann, V. Radical-cation salts of arenes: A new family of organic metals. *Adv. Chem. Ser.* **1988**, *217*, 177–200.
13. Nishinaga, T.; Komatsu, K. Persistent π radical cations: Self-association and its steric control in the condensed phase. *Org. Biomol. Chem.* **2005**, *3*, 5610569. [CrossRef]
14. Krossing, I.; Raabe, I. Noncoordinating anions—fact or fiction? A survey of likely candidates. *Angew. Chem. Int. Ed.* **2004**, *43*, 2066–2090. [CrossRef] [PubMed]
15. Reed, C.A. Carboranes: A new class of weakly coordinating anions for strong electrophiles, oxidants, and superacids. *Acc. Chem. Res.* **1998**, *31*, 133–139. [CrossRef]
16. Grimes, R.N. *Carboranes*, 3rd ed.; Academic Press: Cambridge, MA, USA, 2016.
17. Sivaev, I.; Bregadze, V. Borane, Carborane and Metallacarborane Anions for Stabilization of Transient and Highly Reactive Intermediates: With Applications in Organometallics, Catalysis, Materials and Medicine. In *Handbook of Boron Science. V.1. Boron in Organometallic Chemistry*; Hosmane, N.S., Eagling, R., Eds.; World Scientific Books: London, UK, 2018; pp. 147–203.
18. Fisher, S.P.; Tomich, A.W.; Guo, J.; Lavallo, V. Teaching an Old Dog New Tricks: New Directions in Fundamental and Applied Closo-Carborane Anion Chemistry. *Chem. Commun.* **2019**, *55*, 1684–1701. [CrossRef] [PubMed]
19. Reed, C.A.; Kim, K.S.; Stoyanov, E.S.; Stasko, D.; Tham, F.S.; Mueller, L.J.; Boyd, P.D.W. Isolating benzenium ion salts. *J. Am. Chem. Soc.* **2003**, *125*, 1796–1804. [CrossRef] [PubMed]
20. Müller, T.; Juhasz, M.; Reed, C.A. The X-ray structure of a vinyl cation. *Angew. Chem. Int. Ed.* **2004**, *43*, 1543–1546. [CrossRef] [PubMed]
21. Küppers, T.; Bernhardt, E.; Eujen, R.; Willner, H.; Lehmann, C.W. [Me 3 Si][R-CB 11 F 11]-Synthesis and Properties. *Angew. Chem. Int. Ed.* **2007**, *46*, 6346–6349. [CrossRef] [PubMed]
22. Douglas, T.M.; Molinos, E.; Brayshaw, S.K.; Weller, A.S. Rhodium phosphine olefin complexes of the weakly coordinating anions $[BArF_4]^-$ and $[1\text{-}closo\text{-}CB_{11}H_6Br_6]^-$. Kinetic versus thermodynamic factors in anion coordination and complex reactivity. *Organometallics* **2007**, *26*, 463–465. [CrossRef]
23. Priego, J.L.; Doerrer, L.H.; Rees, L.H.; Green, M.L.H. Weakly-coordinating anions stabilize the unprecedented monovalent and divalent η-benzene nickel cations $[(\eta\text{-}C_5H_5)\text{-}Ni(\eta\text{-}C_6H_6)Ni(\eta\text{-}C_5H_5)]^{2+}$ and $[Ni(\eta\text{-}C_6H_6)_2]^{2+}$. *Chem. Commun.* **2000**, 779–780. [CrossRef]
24. Rosokha, S.V.; Kochi, J.K. Molecular and electronic structures of the long-bonded π-dimers of tetrathiafulvalene cation radical in intermolecular electron transfer and in (solid-state) conductivity. *J. Am. Chem. Soc.* **2007**, *129*, 828–838. [CrossRef]
25. Brown, J.; Zeller, M.; Rosokha, S.V. Effects of structural variations on-dimer formation: Long-distance multicenter bonding of cation-radicals of tetrathiafulvalene analogues *Phys. Chem. Chem. Phys.* **2020**, *22*, 25054–25065. [CrossRef]
26. Brown, J.T.; Grounds, O.; Zeller, M.; Dilley, N.G.; Rosokha, S.V. Structures, multicenter π-bonding, and spin equilibria in the mixed-valence trimers of tetramethyltetrathiafulvalene cation-radicals. *Cryst. Growth Des.* **2021**, *21*, 7257–7268. [CrossRef]
27. Nakayama, S.; Suzuki, K. The electronic absorption spectra of Würster's cation radicals and their dimerization in solution. *Bull. Chem. Soc. Jpn.* **1973**, *46*, 3694–3698. [CrossRef]
28. Sun, D.; Rosokha, S.V.; Kochi, J.K. Donor-acceptor (electronic) coupling in the precursor complex to organic electron transfer: Intermolecular and intramolecular self-exchange between phenothiazine redox centers. *J. Am. Chem. Soc.* **2004**, *126*, 1388–1401. [CrossRef] [PubMed]
29. Lü, J.-M.; Rosokha, S.V.; Kochi, J.K. Stable (long-bonded) dimers via the quantitative self-association of different cationic, anionic, and uncharged π-radicals: Structures, energetics, and optical transitions. *J. Am. Chem. Soc.* **2003**, *125*, 12161–12171. [CrossRef]
30. Hart, H.; Teuerstein, A. Octamethylnaphthalene (improved synthesis) and octamethylbiphenylene. *Synthesis* **1979**, 693–695. [CrossRef]
31. King, B.T.; Noll, B.C.; McKinley, A.J.; Michl, J. Dodecamethylcarba-closo-dodecarboranyl ($CB_{11}Me_{12}\cdot$), a stable free radical. *J. Am. Chem. Soc.* **1996**, *118*, 10902. [CrossRef]
32. Rosokha, S.V.; Stern, C.L.; Ritzert, J.T. π-Bonded molecular wires: Self-assembly of mixed-valence cation-radical stacks within the nanochannels formed by inert tetrakis[3,5-bis(trifluoromethyl)phenyl]borate anions. *CrystEngComm* **2013**, *15*, 10638–10647. [CrossRef]
33. *Bruker (Apex3 v2019.1-0, SAINT V8.40A*, Bruker AXS Inc.: Madison, WI, USA, 2019.
34. *SHELXTL Suite of Programs, Version 6.14, 2000–2003, Bruker Advanced X-ray Solutions*, Bruker AXS Inc.: Madison, WI, USA, 2003.
35. Sheldrick, G. Crystal Structure refinement with SHELXL. *Acta Cryst. C* **2015**, *71*, 3–8. [CrossRef]
36. Sheldrick, G.M. A short history of SHELX. *Acta Crystallogr. A* **2008**, *64*, 112–122. [CrossRef]
37. Hübschle, C.; Sheldrick, G.; Dittrich, B. ShelXle: A Qt Graphical user interface for SHELXL. *J. Appl. Crystallogr.* **2011**, *44*, 1281. [CrossRef]

38. Frisch, M.J.; Trucks, G.W.; Schlegel, H.B.; Scuseria, G.E.; Robb, M.A.; Cheeseman, J.R.; Scalmani, G.; Barone, V.; Mennucci, B.; Petersson, G.A.; et al. *Gaussian 09, Revision C.01*; Gaussian, Inc.: Wallingford, CT, USA, 2009.
39. Zhao, Y.; Truhlar, D.G. The M06 suite of density functionals for main group thermochemistry, thermochemical kinetics, noncovalent interactions, excited states, and transition elements: Two new functionals and systematic testing of four M06-class functionals and 12 other functionals. *Theor. Chem. Acc.* **2008**, *120*, 215–241.
40. Capdevila-Cortada, M.; Ribas-Arino, J.; Novoa, J.J. Assessing the performance of CASPT2 and DFT methods for the description of long, multicenter bonding in dimers between radical ions. *J. Chem. Theory Comput.* **2014**, *10*, 650–658. [CrossRef] [PubMed]
41. Tomasi, J.; Mennucci, B.; Cammi, R. Quantum mechanical continuum solvation models. *Chem. Rev.* **2005**, *105*, 2999. [CrossRef] [PubMed]
42. Cui, Z.; Lischka, H.; Beneberu, H.Z.; Kertesz, M. Rotational barrier in phenalenyl neutral radical dimer: Separating pancake and van der waals interactions. *J. Am. Chem. Soc.* **2014**, *136*, 5539–5542. [CrossRef] [PubMed]
43. Peterson, J.P.; Ellern, A.; Winter, A.H. Spin delocalization, polarization, and London dispersion forces govern the formation of diradical pimers. *J. Am. Chem. Soc.* **2020**, *142*, 5304–5313. [CrossRef] [PubMed]
44. Lu, T.; Chen, F. Multiwfn: A multifunctional wavefunction analyzer. *J. Comput. Chem.* **2012**, *33*, 580–592. [CrossRef]
45. Humphrey, W.; Dalke, A.; Schulten, K. VMD—visual molecular dynamics. *J. Mol. Graph.* **1996**, *14*, 33–38. [CrossRef]
46. Ikemoto, I.; Katagiri, G.; Nishimura, S.; Yakushi, K.; Kuroda, H. Structure of N,N,N′,N′-tetramethyl-p-phenylenediamine. *Acta Cryst. B.* **1979**, *B35*, 2264–2265. [CrossRef]
47. Chu, S.S.C.; van der Helm, D. The refinement of the crystal structure of N-methylphenothiazine *Acta Cryst. B* **1974**, *30*, 2489.
48. Kertesz, M.K. Pancake bonding: An unusual pi-stacking interaction *Chem. -Eur. J.* **2019**, *25*, 400–416. [CrossRef]
49. Preuss, K.E. Pancake bonds: π-Stacked dimers of organic and light-atom radicals. *Polyhedron* **2014**, *79*, 1–15. [CrossRef]
50. Molcanov, K.; Jelsch, C.; Wenger, E.; Mou, Z.; Kertesz, M.; Landeros-Rivera, B.; Hernandez-Trujillo, J.; Stilinovic, V.; Kojic-Prodic, B. Multicentric two-electron covalent bonding (pancake bonding) between semiquinone radicals determines bulk properties. *Acta Crystallogr. Sect. A* **2018**, *74*, E80. [CrossRef]
51. Ganesan, V.; Rosokha, S.V.; Kochi, J.K. Isolation of the latent precursor complex in electron-transfer dynamics. intermolecular association and self-exchange with acceptor anion radicals. *J. Am. Chem. Soc.* **2003**, *125*, 2559–2571. [CrossRef] [PubMed]
52. Xie, Z.; Bau, R.; Reed, C.A. "Free" $[Fe(tpp)]^+$ cation: A new concept in the search for the least coordinating anion. *Angew. Chem. Int. Ed.* **1995**, *33*, 2433–2434. [CrossRef]
53. Rosokha, S.V.; Lu, J.J.; Rosokha, T.Y.; Kochi, J.K. Tris(thianthrene)(2+)-bis(dodecamethylcarba-closo-dodeca bo rate) dichloromethane tetrasolvate: A crossed triple-decker π-trimer dication. *Acta Crystallogr. C* **2007**, *C63*, o347–o349. [CrossRef]
54. Bondi, A. van der Waals volumes and radii. *J. Phys. Chem.* **1964**, *68*, 441–451. [CrossRef]